Electronic Interactions in (η^6-Arene) Ferracarboranes[1]

Fabrizia Fabrizi de Biani,[†] Marco Fontani,[†] Eliseo Ruiz,[‡] Piero Zanello,*[,†] J. Monte Russell,[§] and Russell N. Grimes*[,§]

Dipartimento di Chimica dell'Università di Siena, Via Aldo Moro, 53100 Siena, Italy, Departament de Química Inorgànica, Universitat de Barcelona, Diagonal, 647, 08028 Barcelona, Spain, and Department of Chemistry, University of Virginia, Charlottesville, Virginia 22901

Received February 25, 2002

The electronic structures of a series of di- and trinuclear ferracarboranes that incorporate FeC_2B_4 cluster units connected by aryl, heterocyclic, or alkynyl bridges or via direct intercluster B−B bonding have been explored by cyclic voltammetry, controlled-potential coulometry, and DFT and PM3 molecular orbital calculations. The data reflect the strong electron-donating properties of the $Et_2C_2B_4H_4^{2-}$ carborane ligand; thus, in the ferrocenyl derivative (η^6-C_6H_6)Fe($Et_2C_2B_4H_3$-5-Fc) there is a substantial flow of electron density from the ferracarborane cluster to the ferrocenyl moiety. In all complexes examined, one or more reversible oxidations of Fe^{II} to Fe^{III} centers were observed, with varying degrees of separation of successive $E°$ values, indicating a range of electron-delocalization behavior. In many of the observed mixed-valent Fe^{II}−Fe^{III} species the evidence suggests little or no metal−metal communication, paralleling earlier studies of small arene-ferracarboranes; however, significant delocalization is evidently present in the thiophene-bridged cation 2,5-[(η^6-C_6H_6)Fe($Et_2C_2B_4H_3$-5-)]$_2SC_4H_2^+$ (**10**$^+$). Although the asymmetric dimer (η^6-C_6H_6)Fe($Et_2C_2B_4H_3$-5-)(η^6-C_6H_5)Fe($Et_2C_2B_4H_4$)$^+$ (**4**$^+$) exhibits a large (0.56 V) separation between oxidation processes, implying that **4**$^+$ is a fully delocalized Robin−Day class III system, detailed MO calculations on the latter species show that this $\Delta E°$ value results from inequivalence in the electronic environments of the two iron centers, rather than from electron delocalization between them.

Introduction

Recent papers[1b,2] from one of our groups have described the synthesis of families of covalently bound aryl- and alkynyl-linked polymetallacarboranes that incorporate MC_2B_4 clusters, where M in most cases is Fe, Co, or Ta. These multinuclear complexes exhibit several characteristics that make them potential building blocks for advanced electronic materials:[3] with few exceptions they are air-stable crystalline solids, soluble in organic solvents, that can be functionalized at desired cage vertexes. Typically, *they retain their structural integrity upon oxidation or reduction*. However, the development of such applications requires detailed information on the electronic structures and properties of these systems, with particular attention to the influence of substituents, metal oxidation states, and molecular architecture on electron delocalization between metal centers. Insofar as the MC_2B_4 and MC_2B_3 small-cluster systems are concerned, detailed electrochemical studies of bis(cobaltacarboranes) and bis(ferracarboranes),[4] and of iron, cobalt, and ruthenium arylmetallacarboranes,[5] have been conducted. Related electrochemical and ESR studies have dealt with multidecker sandwich complexes based on seven-vertex MC_2B_3M' cluster units,[5e,6] including "staircase" oligomers that feature tetradecker sandwich repeating units.[7]

In an earlier electrochemical investigation of mononuclear (arene)ferracarboranes by Merkert et al.,[5a,b] the $Et_2C_2B_4H_4^{2-}$ ligand was demonstrated to exert a strong stabilizing influence via electron donation to the metal, in (arene)$M^{III}(Et_2C_2B_4H_4)^+$ complexes of iron and ruthenium. This behavior contrasts sharply with that of their highly unstable organometallic (arene)$M^{III}(C_5R_5)^{2+}$

[†] Università di Siena.
[‡] Universitat de Barcelona.
[§] University of Virginia.

(1) (a) Organotransition-Metal Metallacarboranes. 60. (b) Part 59: Russell, J. M.; Sabat, M.; Grimes, R. N. *Organometallics* **2002**, *21*, 4113.

(2) (a) Malaba, D.; Sabat, M.; Grimes, R. N. *Eur. J. Inorg. Chem.* **2001**, 2557. (b) Bluhm, M.; Pritzkow, H.; Siebert, W.; Grimes, R. N. *Angew. Chem., Int. Ed.* **2000**, *39*, 4562; *Angew. Chem.* **2000**, *112*, 4736. (c) Stockman, K. E.; Boring, E. A.; Sabat, M.; Finn, M. G.; Grimes, R. N. *Organometallics* **2000**, *19*, 2200. (d) Curtis, M. A.; Müller, T.; Beez, V.; Pritzkow, H.; Siebert, W.; Grimes, R. N. *Inorg. Chem.* **1997**, *36*, 3602. (e) Boring, E. A.; Sabat, M.; Finn, M. G.; Grimes, R. N. *Organometallics* **1998**, *17*, 3865.

(3) (a) Grimes, R. N. In *Contemporary Boron Chemistry*; Davidson, M., Hughes, A. K., Marder, T. B., Wade, K., Eds.; Royal Society of Chemistry: London, 2000; pp 283−290. (b) Grimes, R. N. *Appl. Organomet. Chem.* **1996**, *10*, 209.

(4) (a) Chin, T. T.; Grimes, R. N.; Geiger, W. E. *Inorg. Chem.* **1999**, *38*, 93. (b) Chin, T. T.; Lovelace, S. R.; Geiger, W. E.; Davis, C. M.; Grimes, R. N. *J. Am. Chem. Soc.* **1994**, *116*, 9359.

(5) (a) Merkert, J. M.; Geiger, W. E.; Davis, J. H., Jr.; Attwood, M. D.; Grimes, R. N. *Organometallics* **1989**, *8*, 1580. (b) Merkert, J. M.; Geiger, W. E.; Attwood, M. D.; Grimes, R. N. *Organometallics* **1991**, *10*, 3545. (c) Fessenbecker, A.; Stephan, M.; Grimes, R. N.; Pritzkow, H.; Zenneck, U.; Siebert, W. *J. Am. Chem. Soc.* **1991**, *113*, 3061. (d) Stephan, M.; Davis, J. H., Jr.; Meng, X.; Chase, K. P.; Hauss, J.; Zenneck, U.; Pritzkow, H.; Siebert, W.; Grimes, R. N. *J. Am. Chem. Soc.* **1992**, *114*, 5214. (e) Merkert, J.; Davis, J. H., Jr.; Geiger, W.; Grimes, R. N. *J. Am. Chem. Soc.* **1992**, 114, 9846. (f) Stephan, M.; Hauss, J.; Zenneck, U.; Siebert, W.; Grimes, R. N. *Inorg. Chem.* **1994**, *33*, 4211.

10.1021/om0201617 CCC: $22.00
Publication on Web 08/24/2002

analogues,[8] where R = H, Me. (Arene)$M^{I}(Et_2C_2B_4H_4)^-$ monoanions, on the other hand, are *de*stabilized by the carborane ligand but are sufficiently persistent to allow characterization by ESR spectroscopy.[5b] In all cases studied, the evidence suggested that the singly occupied molecular orbitals (SOMOs) in these complexes are similar to those of (arene)$M(C_5R_5)$ systems.

Examination of the hydrocarbon-bridged dinuclear complexes $[(Et_2C_2B_4H_4)Fe^{II}]_2(C_6H_5)_2$ (**Fe_2**) and $(Et_2C_2B_4H_4)Co^{III}]_2(C_5H_4)_2$ (**Co_2**) via IR spectroelectrochemistry[4] revealed that the oxidized monocation **Fe_2^+** is a trapped-valence d^6d^5 $Fe^{II}-Fe^{III}$ complex while the reduced monoanion **Co_2^-** (a d^6d^7 system) is a fully delocalized $Co^{2.5}-Co^{2.5}$ species. These findings, together

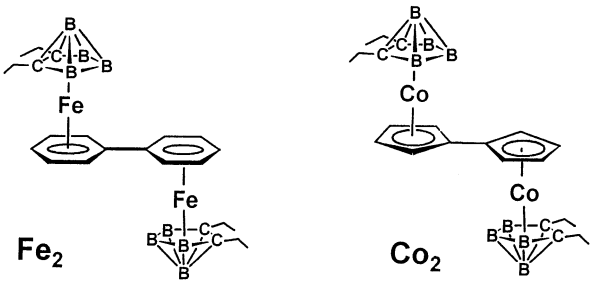

with other work cited above, demonstrate that polynuclear metallacarboranes exhibit a wide range of electronic behavior that is strongly dependent on structure and composition. In the present work we explore a series of di- and trinuclear ferracarborane linked systems and attempt to cast light on some unexplained features of earlier studies.

Experimental Section

Electrochemistry. Anhydrous 99.9% HPLC grade dichloromethane for electrochemistry was purchased from Aldrich. The supporting electrolyte used was electrochemical grade $[NBu_4]PF_6$ obtained from Fluka. Cyclic voltammetry was performed in a three-electrode cell having a platinum working electrode surrounded by a platinum-spiral counter electrode and an aqueous saturated calomel reference electrode (SCE) mounted with a Luggin capillary. Either a BAS 100A or a BAS 100W electrochemical analyzer was used as a polarizing unit. Controlled-potential coulometry was performed in an H-shaped cell with anodic and cathodic compartments separated by a sintered-glass disk. The working macroelectrode was platinum gauze; a mercury pool was used as the counter electrode. All reported potential values are referenced to the saturated calomel electrode (SCE).

Computational Methods. The Spartan[9] program was used for PM3[10] semiempirical calculations. DFT calculations were carried out with the Gaussian98 package,[11] using the hybrid B3LYP method proposed by Becke.[12] An all-electron double-ζ basis set has been used for carbon, boron, and hydrogen atoms[13] and a triple-ζ basis set, including two polarization p functions, for iron atoms.[14] Owing to the large dimensions of the systems, no attempt was made to optimize the geometry of the dimers at the DFT level, while the full geometry optimization was accomplished for the monomer **1a** by using both DFT and PM3 semiempirical methods. Employing two different methods enabled us to assess their performance in predicting both the molecular and electronic structure of this complex. In Table S-1 (Supporting Information) we compare the optimized geometry of **1a** with that determined from X-ray crystallography.[15] Since the crystals of **1a** contain two independent molecules (a and b in Figure S-1, Supporting Information), the more relevant geometric parameters of both are reported in Table S-1. For molecules a and b, respectively, the average deviation between the calculated and experimental bond lengths is 0.04−0.06 Å for PM3 and 0.01−0.03 Å for DFT. The higher absolute deviation is 0.14 Å for the PM3 prediction of the distance between the capping boron and the centroid of the B_3C_2 ring (Ct1). The Ct1−Fe−Ct2 bond angle is also accurately reproduced, the deviation being 2.3−2.7 and 0.0−0.4° for PM3 and DFT optimized structures, respectively. Thus, the DFT optimized structure is in very good agreement with the experimental data, while PM3 predicts bond lengths and angles of comparable quality. This allowed us to confidently use the PM3 optimized structures of **4**−**6** and **11**, for which X-ray structures are not available. On this basis, the DFT calculations thereafter were performed on the PM3 optimized structures. Calculations using the broken-symmetry formalism[16] were carried out for the cationic species. Due to the high computational effort required by these calculations, which is doubled by the spin-unrestricted approach, the PM3-optimized geometry calculated for the neutral species has been kept unchanged for the charged ones.

Results and Discussion

Electrochemical Data. The structures of the complexes examined in this study are shown in Charts 1 and 2, while the electrode potentials of their redox changes are listed in Table 1. In dichloromethane solution the B(5)−phenyl derivative (η^6-C_6H_6)Fe^{II}-

(6) (a) Brennan, D. E.; Geiger, W. E., Jr. *J. Am. Chem. Soc.* **1979**, *101*, 3399. (b) Fessenbecker, A.; Attwood, M. D.; Bryan, R. F.; Grimes, R. N.; Woode, M. K.; Stephan, M.; Zenneck, U.; Siebert, W. *Inorg. Chem*. **1990**, *29*, 5157. (c) Fessenbecker, A.; Attwood, M. D.; Grimes, R. N.; Stephan, M.; Pritzkow, H.; Zenneck, U.; Siebert, W. *Inorg. Chem*. **1990**, *29*, 5164. (d) Chase, K. J.; Bryan, R. F.; Woode, M. K.; Grimes, R. N. *Organometallics* **1991**, *10*, 2631. (e) Stockman, K. E.; Sabat, M.; Finn, M. G.; Grimes, R. N. *J. Am. Chem. Soc.* **1992**, *114*, 8733. (f) Pipal, J. R.; Grimes, R. N. *Organometallics* **1993**, *12*, 4452. (g) Stephan, M.; Mueller, P.; Zenneck, U.; Pritzkow, H.; Siebert, W.; Grimes, R. N. *Inorg. Chem*. **1995,** *34*, 2058. (h) Stockman, K. E.; Houseknecht, K. L.; Boring, E. A.; Sabat, M.; Finn, M. G.; Grimes, R. N. *Organometallics* **1995**, *14*, 3014. (i) Wang, X.; Sabat, M.; Grimes, R. N. *J. Am. Chem. Soc.* **1995**, *117*, 12218, 12227. (j) Curtis, M. A.; Houser, E. J.; Sabat, M.; Grimes, R. N. *Inorg. Chem*. **1998**, *37*, 102.

(7) Pipal, J. R.; Grimes, R. N. *Organometallics* **1993**, *12*, 4459.

(8) (a) Nesmeyanov, A. N.; Vol'kenau, N. A.; Sirotkina, E. I.; Deryabin, V. V. *Dokl. Akad. Nauk SSSR* **1967**, *177*, 1170 (English), 1110 (Russian). (b) Nesmeyanov, A. N.; Vol'kenau, N. A.; Sirotkina, E. I. *Izv. Akad. Nauk SSSR* **1967**, 1142 (English), 1170 (Russian). (c) Morrison, W. H., Jr.; Ho, E. Y.; Hendrickson, D. N. *J. Am. Chem. Soc.* **1974**, *96*, 3603. (d) Astruc, D. *Tetrahedron* **1983**, *39*, 4027.

(9) SPARTAN 5.1; Wavefunction, Inc., 18401 Von Karman Ave., Suite 370, Irvine, CA 92612.

(10) Stewart, J. J. P. *J. Comput. Chem*. **1989**, *10*, 209.

(11) Frisch, M. J.; Trucks, G. W.; Schlegel, H. B.; Scuseria, G. E.; Robb, M. A.; Cheeseman, J. R.; Zakrzewski, V. G.; Montgomery, J. A., Jr.; Stratmann, R. E.; Burant, J. C.; Dapprich, S.; Millam, J. M.; Daniels, A. D.; Kudin, K. N.; Strain, M. C.; Farkas, O.; Tomasi, J.; Barone, V.; Cossi, M.; Cammi, R.; Mennucci, B.; Pomelli, C.; Adamo, C.; Clifford, S.; Ochterski, J.; Petersson, G. A.; Ayala, P. Y.; Cui, Q.; Morokuma, K.; Malick, D. K.; Rabuck, A. D.; Raghavachari, K.; Foresman, J. B.; Cioslowski, J.; Ortiz, J. V.; Stefanov, B. B.; Liu, G.; Liashenko, A.; Piskorz, P.; Komaromi, I.; Gomperts, R.; Martin, R. L.; Fox, D. J.; Keith, T.; Al-Laham, M. A.; Peng, C. Y.; Nanayakkara, A.; Gonzalez, C.; Challacombe, M.; Gill, P. M. W.; Johnson, B. G.; Chen, W.; Wong, M. W.; Andres, J. L.; Head-Gordon, M.; Replogle, E. S.; Pople, J. A. *Gaussian 98*, revision A.9; Gaussian, Inc.: Pittsburgh, PA, 1998.

(12) Becke, A. D. *J. Chem. Phys*. **1993**, *98*, 5648.

(13) Schafer, A., Horn, H.; Ahlrichs, R. *J. Chem. Phys*. **1992,** *97*, 2571.

(14) Schafer, A.; Huber, C.; Ahlrichs, R. *J. Chem. Phys*. **1994**, *100*, 5829.

(15) Swisher, R. G.; Sinn, E.; Grimes, R. N. *Organometallics* **1983**, *2*, 506.

(16) (a) Noodleman, L.; Norman, J. G. *J. Chem. Phys.* **1979**, *70*, 4903. (b) Noodleman, L., *J. Chem. Phys*. **1981**, *74*, 5737. (c) Noodleman, L.; Case, D. A. *Adv. Inorg. Chem*. **1992**, *38*, 423.

Chart 1[a]

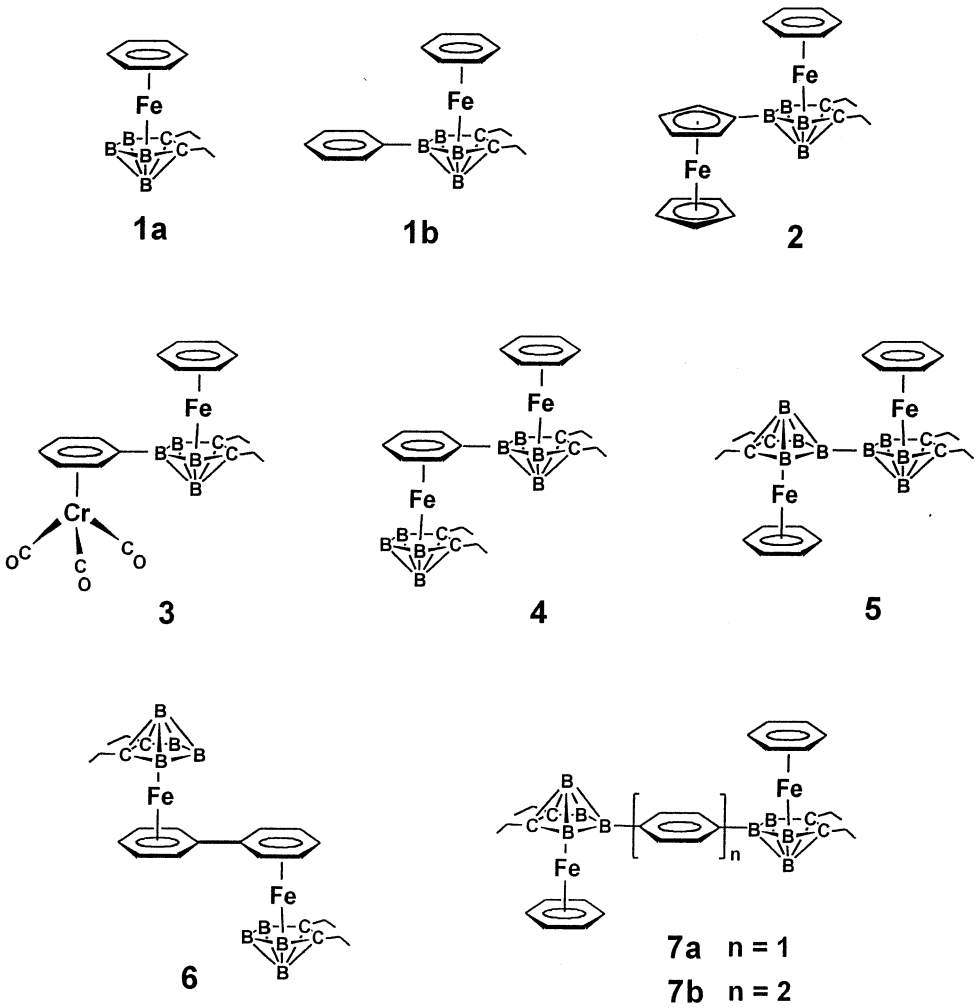

[a] B = BH, B.

($Et_2C_2B_4H_3$-5-Ph) (**1b**; Chart 1) shows a reversible one-electron oxidation at $E° = +0.93$ V that is similar to that of the parent species (η^6-C_6H_6)Fe^{II}($Et_2C_2B_4H_4$) (**1a**) ($E° = +1.01$ V).[5a,b]

Analysis[17] of the cyclic voltammograms with scan rates varying from 0.02 to 2.0 V s^{-1} is diagnostic for a simple Fe(II)/Fe(III) electron transfer ($i_{p,c}/i_{p,a} = 1$; ΔE_p close to the theoretical value of 60 mV; $i_{p,a}v^{-1/2}$ constant). However, in controlled-potential coulometry ($E_w = +1.1$ V), the electrogenerated brown-yellow Fe(III) monocation **1b**$^+$ slowly rereduces to the neutral yellow Fe(II) species **1b**, probably because of reaction with traces of water present in the nominally anhydrous solvent.

Attachment of a ferrocenyl unit to the ferracarborane framework as in complex **2**[1b] gives rise, as expected, to two anodic processes: a ferrocene-centered one-electron oxidation that is reversible in character, and a subsequent ferracarborane-centered one-electron removal (Figure 1). The first, ferrocene-centered oxidation ($E_w = +0.4$ V) was shown by controlled-potential coulometry to consume one electron per molecule. The original yellow-orange solution turned brown upon oxidation and displayed a cyclic voltammetric profile quite complementary to that of the neutral congener. Since iron-centered ferrocenium ions usually assume a blue-to-green color, the fact that the monocation **2**$^+$ is brown implies that the HOMO of **2** is significantly affected by the ferracarborane unit. In support of this idea, the oxidation of the ferrocenyl unit in **2** occurs at a potential less positive by 0.26 V with respect to free ferrocene (Table 1), whereas the oxidation of the ferracarborane unit occurs at a potential more positive by 0.14 V than that of **1a**. From these data we infer that there is a significant transfer of electron density from the ferracarborane to the ferrocenyl unit.

The substitution of a (C_6H_5)$Cr(CO)_3$ fragment for H on B(5) in **1a,** generating **3**,[1b] also affords two separated oxidation processes (Figure 2). In this case, however, the voltammetric profile shows evidence of chemical degradation of the oxidized species, probably reflecting the well-known instability of the (C_6H_6)$Cr(CO)_3^+$ monocation.[18] As a matter of fact, despite the apparent chemical reversibility of the **3**/**3**$^+$ redox change on the cyclic voltammetric time scale, exhaustive electrolysis ($E_w = +0.8$ V) causes partial decomposition of **3**$^+$, as proved by cyclic voltammetric tests performed on the resulting solution. Here again it is notable that the oxidation of the chromium unit occurs at a potential

(17) Brown, E. R.; Sandifer, J. R. In *Physical Methods of Chemistry*, Rossiter, B. W., Hamilton, J. F., Eds.; Wiley: New York, 1986; Vol. 2 (Electrochemical Methods), Chapter 4.

(18) Zoski, C. G.; Sweigart, D. A.; Stone, N. J.; Rieger, P. H.; Mocellin, E.; Mann, T. F.; Mann, D. R.; Gosser, D. K.; Doeff, M. M.; Bond, A. M. *J. Am. Chem. Soc.* **1988**, *110*, 2109.

Chart 2[a]

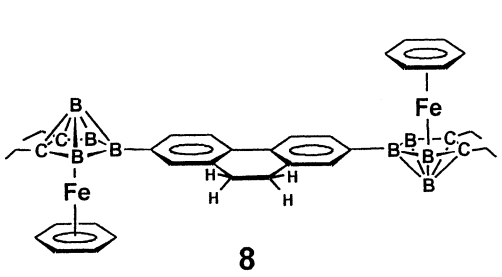

8

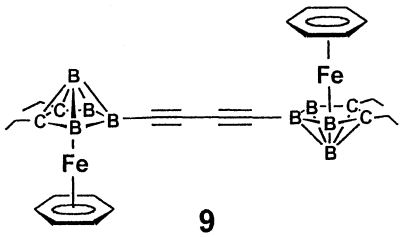

9

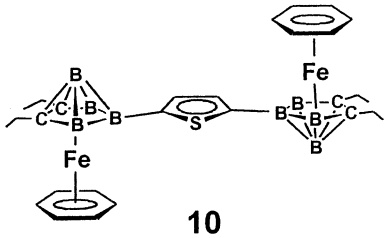

10

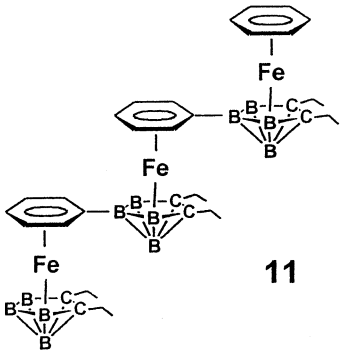

11

[a] B = BH, B.

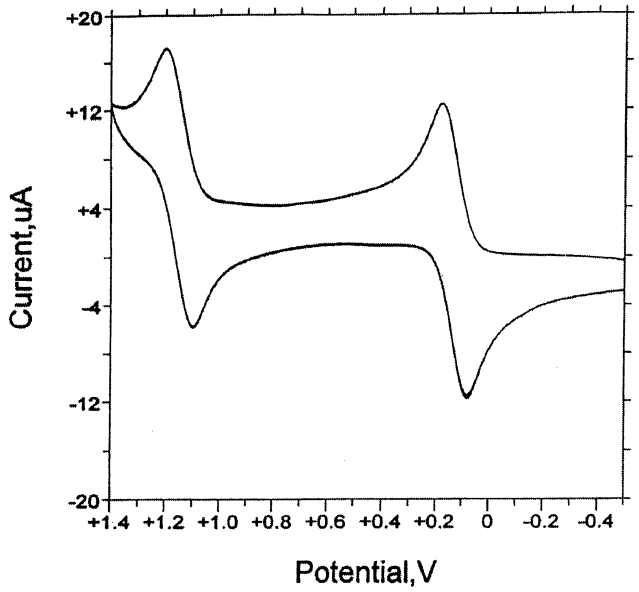

Figure 1. Cyclic voltammetric response recorded at a platinum electrode on a CH_2Cl_2 solution of **2** (0.8×10^{-3} mol dm^{-3}). $[NBu_4]PF_6$ (0.2 mol dm^{-3}) was used as supporting electrolyte, and the scan rate was 0.1 V s^{-1}.

value less positive by 0.22 V than that of free $(C_6H_6)Cr(CO)_3$, while the potential of the ferracarborane cluster is 0.22 V higher than that of the parent ferracarborane **1a** (Table 1), again indicating substantial electron donation from the carborane to the $Cr(CO)_3$ moiety.

Turning now to the asymmetric bis(ferracarborane) complex **4**, its cyclic voltammogram (Figure 3) shows two discrete one-electron oxidations, both possessing features of chemical reversibility. Such behavior is somewhat reminiscent of that exhibited by the biphenyl−bis(ferracarborane) complex **6**,[5a] which afforded two successive oxidations separated by 0.29 V. In **4**, the rather large 0.56 V separation between the two oxidation processes implies that the electronic interaction between the two ferracarborane subunits is greater in **4** than in **6**. Thus, the K_{com} value of 3×10^9 of the mixed-valence species $\mathbf{4}^+$ would appear to identify it as a completely delocalized Robin−Day class III species, whereas $\mathbf{6}^+$ ($K_{com} = 8 \times 10^4$) belongs to the partially delocalized class II. However, these conclusions are in part misleading, as will be seen from theoretical calculations discussed below.

More complex behavior is exhibited by the symmetric B−B-connected complex **5**. As shown in Figure 4, at low scan rate (Figure 4, plot a) this compound exhibits a single oxidation at about +0.5 V that is accompanied by chemical complications, affording an anodic peak at about +0.7 V and a return peak at about 0 V. In fact, controlled-potential coulometry ($E_w = +0.8$ V) reveals that two electrons are consumed per molecule. However, as illustrated in the sequence of plots b−d in Figure 4, the increase in the scan rate competes with the chemical complications; thus, a return peak directly associated with the first anodic step appears concomitantly with the clear appearance of a second oxidation process. At the same time the current function $i_p v^{-1/2}$ of the first oxidation decreases from 2.3 at 0.02 V s^{-1} to 1.4 at 2.0 V s^{-1}, indicating a decrease in the number of electrons involved in the first oxidation step. These data hence support the hypothesis that the oxidation of **5** proceeds through two separate one-electron processes in which both the monocation $\mathbf{5}^+$ and the dication $\mathbf{5}^{2+}$ are significantly unstable.

Let us now examine the bis(ferracarborane) complexes in which different groups are interposed between the two iron subunits. As illustrated in Figure 5, two partially overlapping oxidations appear in the cyclic voltammogram of the phenyl-bridged complex **7a**, both having features of chemical reversibility. Comparison with the response obtained using an equimolar amount of decamethylferrocene as an internal standard ($E^{o\prime}_{0/+}$

Table 1. Formal Electrode Potentials (in V, vs SCE) and Peak-to-Peak Separations (in mV) for (η^6-Benzene)ferracarborane Complexes in Dichloromethane Solution

	$Fe^{II/III}$ step(s) for ferracarborane units						1e oxidns of metallo substituents		
complex	$E^{\circ\prime}_{first}$	ΔE_p[a]	$E^{\circ\prime}_{second}$	ΔE_p[a]	$E^{\circ\prime}_{third}$	ΔE_p[a]	$E^{\circ\prime}$	ΔE_p[a]	ref
1a	+1.01								5a,b
1b	+0.93	82							*b*
2	+1.15	100					+0.13	90	*b*
3	+1.23[a,c]						+0.58	71	*b*
4	+0.63	67	+1.19	70					*b*
5	+0.56	100[d]	+0.76[e]						*b*
6	+1.02		+1.31						5a
7a	+0.82	*f*	+0.92	*f*					*b*
7b	+0.90	100	+0.90	100					*b*
8	+0.86	109	+0.86	109					*b*
9	+1.00	70	+1.00	70					*b*
10	+0.67	75	+0.99	120[d]					*b*
11	+0.56	60	+0.93	60	+1.25	62			*b*
FcH							+0.39	85	*b*
$(C_6H_6)Cr(CO)_3$							+0.80		17

[a] Measured at 0.1 V s^{-1}. [b] Present work. [c] Peak potential value. [d] Measured at 0.5 V s^{-1}. [e] Measured at 2.0 V s^{-1}. [f] Difficult to evaluate.

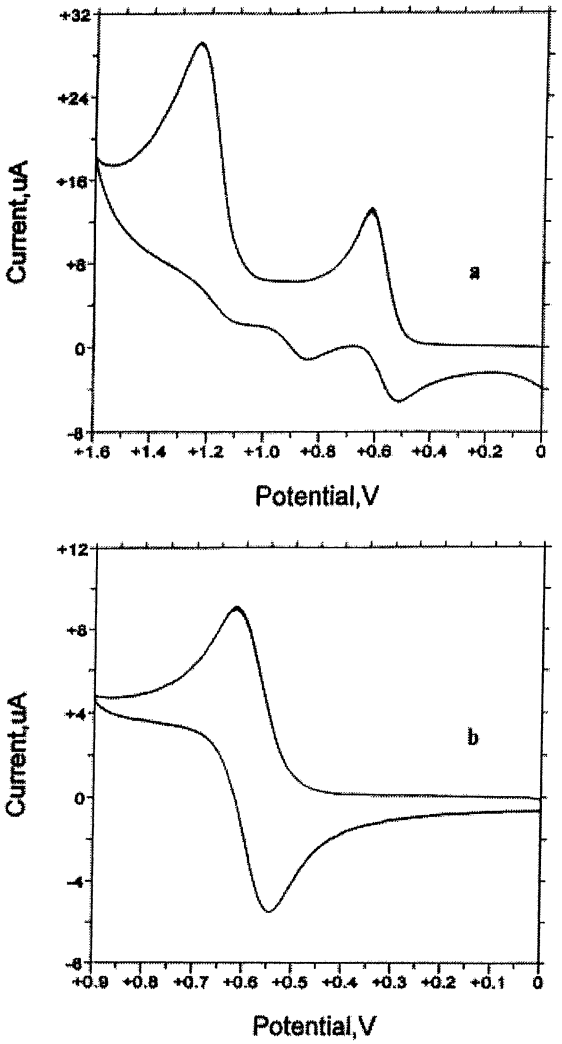

Figure 2. Cyclic voltammetric responses recorded at a platinum electrode on a CH_2Cl_2 solution of **3** (0.6×10^{-3} mol dm^{-3}). $[NBu_4]PF_6$ (0.2 mol dm^{-3}) was used as supporting electrolyte, and the scan rates (V s^{-1}) were (a) 0.2 and (b) 0.1.

= −0.13 V) supports the one-electron nature of each step. As shown, the two processes become sufficiently well separated in differential pulse voltammetry (DPV) to reveal a separation of 0.1 V between them. This

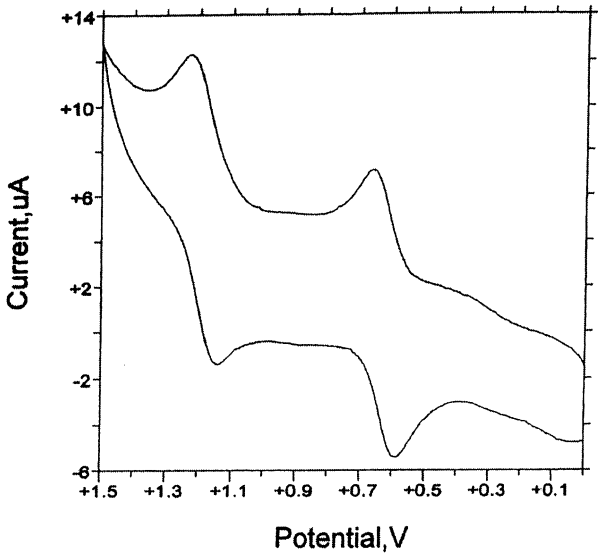

Figure 3. Cyclic voltammetric response recorded at a platinum electrode on a CH_2Cl_2 solution of **4** (0.5×10^{-3} mol dm^{-3}). $[NBu_4]PF_6$ (0.2 mol dm^{-3}) was used as supporting electrolyte, and the scan rate was 0.05 V s^{-1}.

indicates that in **7a** the presence of the interposed phenyl ring stabilizes the oxidation products but significantly attenuates the electronic interaction between the two iron subunits in comparison to **5**, whose carborane units are directly linked via an intercage B−B bond. In **7b** the insertion of two phenyl rings between the ferracarborane units results in a single two-electron oxidation (Figure 6); no separation is evident in DPV, signifying the absence of any measurable electronic interaction between the two metal centers.

A similar electronic effect is produced when the intercage linking group is a 9,10-dihydrophenanthrene group as in **8** or a diacetylene chain as in **9** (structures shown in Chart 2). In both cases a single two-electron oxidation, which is unresolved either in DPV or OSWV (Osteryoung square wave voltammetry), is observed, again indicating noncommunication between the iron atoms.

Figure 7 depicts the cyclic voltammetric behavior exhibited by the thiophene-bridged complex **10**, in which two discrete oxidations appear. At low scan rates (Figure

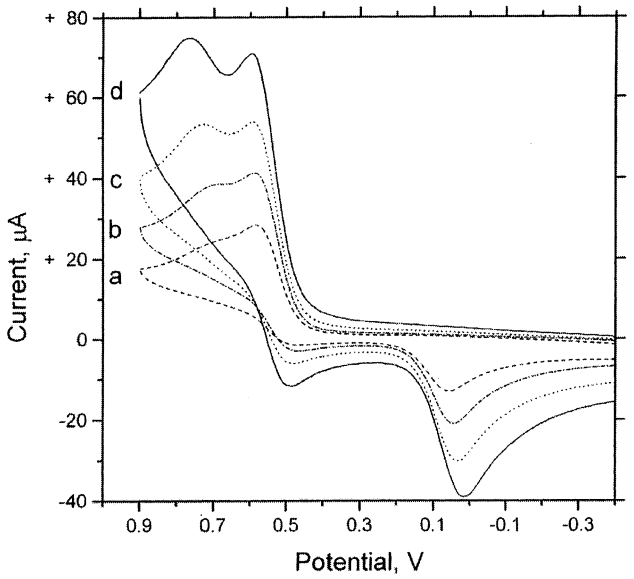

Figure 4. Cyclic voltammetric responses recorded at a platinum electrode on a CH_2Cl_2 solution of **5** (0.3×10^{-3} mol dm^{-3}). $[NBu_4]PF_6$ (0.2 mol dm^{-3}) was used as supporting electrolyte, and the scan rates (V s^{-1}) were (a) 0.2, (b) 0.5, (c) 1.0, and (d) 2.0.

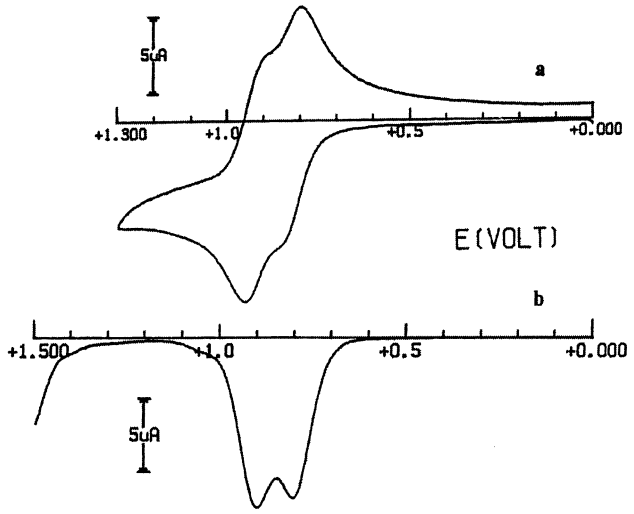

Figure 5. Cyclic and differential pulse voltammetric responses recorded at a platinum electrode on a CH_2Cl_2 solution of **7a** (0.8×10^{-3} mol dm^{-3}). $[NBu_4]PF_6$ (0.2 mol dm^{-3}) was used as supporting electrolyte, and the scan rates (V s^{-1}) were (a) 0.1 and (b) 0.07.

7a) the data indicate that the first oxidation is associated with chemical complications that cause the current of the second wave to approximately double, whereas at high scan rates (Figure 7b) the two processes are of equal intensity and display features of complete chemical reversibility. In fact, the analysis of the first step with scan rates varying from 0.02 to 1.00 V s^{-1} shows that the $i_{p,c}/i_{p,a}$ ratio progressively increases from 0.6 to 1.0. As a first hypothesis, we assume that the first one-electron removal causes slow fragmentation of the molecule, leading to the regeneration of the parent species **1a**. Despite the instability of the monocation, it is noteworthy that the separation of the two processes is 0.32 V, notably higher than that present in **7a**; hence, it appears that the thiophene spacer allows a greater degree of electronic communication between the two ferracarborane subunits than does a phenylene unit.

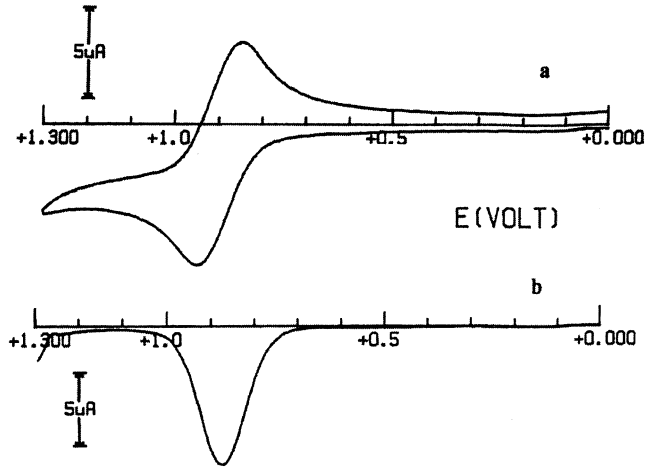

Figure 6. Cyclic voltammetric response recorded at a platinum electrode on a CH_2Cl_2 solution of **7b** (0.4×10^{-3} mol dm^{-3}). $[NBu_4]PF_6$ (0.2 mol dm^{-3}) was used as supporting electrolyte, and the scan rate was 0.1 V s^{-1}.

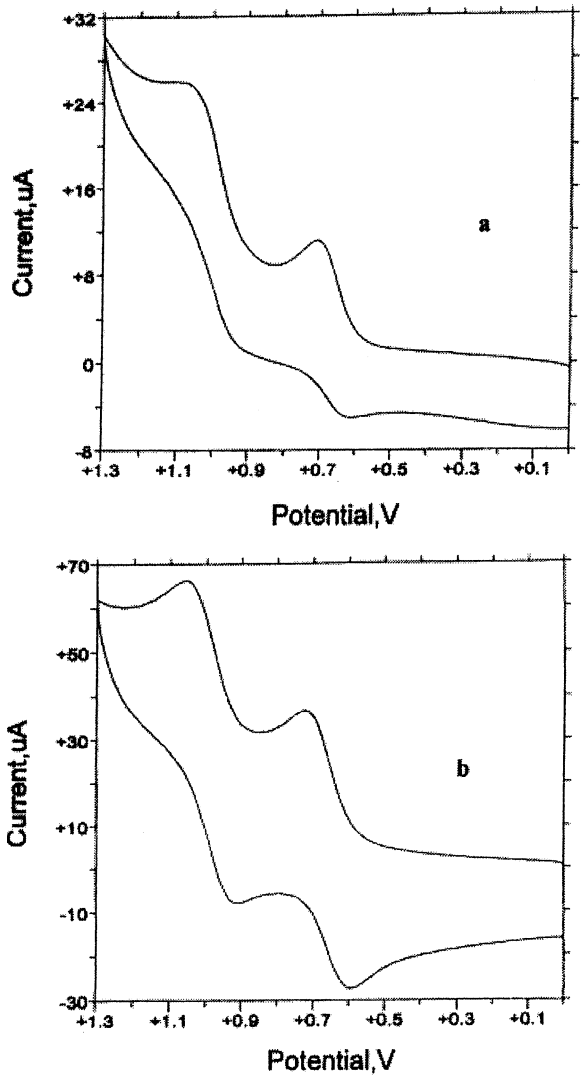

Figure 7. Cyclic voltammetric responses recorded at a platinum electrode on a CH_2Cl_2 solution of **10** (0.9×10^{-3} mol dm^{-3}). $[NBu_4]PF_6$ (0.2 mol dm^{-3}) was used as supporting electrolyte, and the scan rates (V s^{-1}) were (a) 0.2 and (b) 2.0.

Finally, Figure 8 shows the cyclic voltammetric response exhibited by the trinuclear complex **11** in

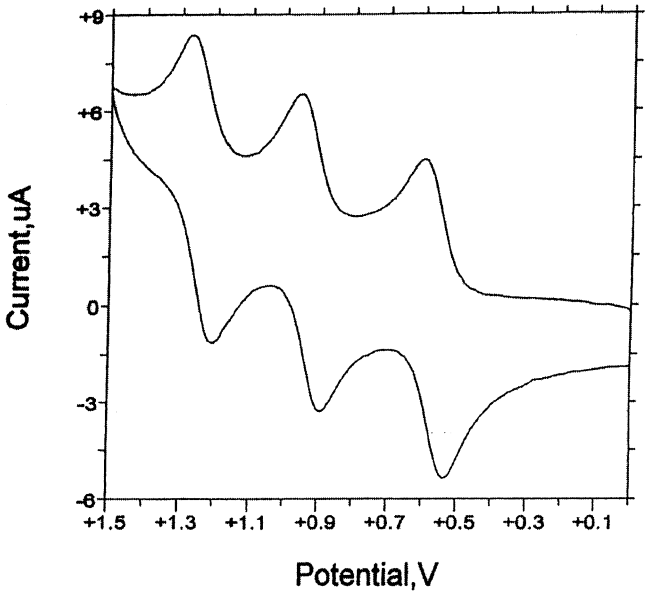

Figure 8. Cyclic voltammetric response recorded at a platinum electrode on a CH_2Cl_2 solution of **11** (0.7×10^{-3} mol dm^{-3}). $[NBu_4]PF_6$ (0.2 mol dm^{-3}) was used as supporting electrolyte, and the scan rate was 0.1 V s^{-1}.

dichloromethane solution. As seen, three well-separated oxidation processes occur, all indicative of chemical reversibility on the cyclic voltammetric time scale. Controlled-potential coulometry performed in correspondence to the first anodic step confirmed the one-electron nature of the electron transfer. In addition, cyclic voltammetric tests performed after the exhaustive one-electron oxidation (during which the original yellow solution turns brown) established the complete chemical reversibility of the **11**/**11**$^+$ redox change, in that the voltammetric profiles are quite complementary to the original ones. We did not succeed in carrying out the exhaustive oxidation at the subsequent anodic steps **11**$^+$/**11**$^{2+}$/**11**$^{3+}$, owing to a slow rereduction of the oxidized species which prevented completion of the processes; at any rate no irreversible fragmentation was observed in the course of these controlled-potential tests. The behavior of complexes **4** and **11** reveals a similarity between the present ferracarboranes and ferrocenes, in that biferrocene and triferrocene also display two and three separated reversible oxidations, respectively.[19]

Molecular Orbital Calculations. As we have seen, several of the ferracarboranes studied exhibit two or more redox processes. Of particular interest is the behavior of the dimeric complexes **4**−**6** compared with that of the trimeric **11**. As noted earlier, **4**−**6** undergo two separate oxidations and the trimer **11** exhibits three oxidation steps. In general, the observation of multiple redox processes can arise from dissimilar electronic environments at the different redox centers and/or as a consequence of electronic communication between the centers. In complexes **4** and **11** the iron atoms occupy electronically different sites; hence, either of these factors could be responsible for the observed splitting. In an effort to interpret the redox behavior of these systems, we have undertaken a theoretical analysis of their electronic structure.

(19) Brown, G. M.; Meyer, T. J.; Cowan, D. O.; LeVanda, C.; Kaufman, F.; Roling, P. V.; Rausch, M. D. *Inorg. Chem.* **1975**, *14*, 506.

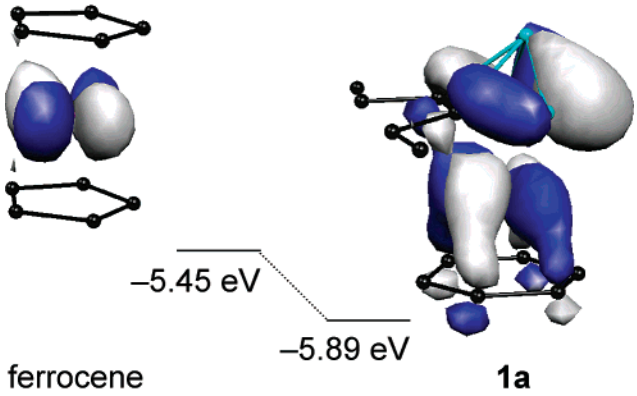

Figure 9. Energies and shapes of the highest occupied molecular orbitals of ferrocene and **1a**, as obtained from B3LYP calculations.

First, we addressed the question of why the redox change **1a**/**1a**$^+$ ($E° = +1.01$ V) occurs at potential values more positive by 0.6 V than the ferrocene/ferrocenium couple ($E° = +0.39$ V). According to our calculations, while the HOMO in ferrocene is a nonbonding iron-centered orbital, the HOMO in **1a** has a major contribution from the $[R_2C_2B_4H_4]^{2-}$ unit, which has an antibonding interaction with the iron d_{xy} orbital and a minor bonding contribution from the π^* orbital of benzene (Figure 9). Although the latter contribution is small, it is sufficient to stabilize the HOMO energy in **1a** with respect to ferrocene ($\Delta E = 0.44$ eV), thus accounting for the fact that **1a** is more difficult to oxidize. On the basis of these features one would expect strong substitution effects, which are indeed found. As reported above, in the absence of any metal-to-metal interactions, the simple introduction of a phenyl unit, as in complex **1b**, gives rise to a cathodic shift relative to **1a**.

To assess the reliability of the method used, we calculated the redox potentials for the first oxidations of complexes **1a**, **4**−**6**, and **11** as a function of the relative energy of the HOMOs, as follows. The potential for a one-electron redox change X/X$^+$ can be expressed as

$$E°_{NHE} = \Delta G^{ox}{}_{sol}\,(\text{eV})$$

where

$$\Delta G^{ox}{}_{sol} = \Delta G^{ox}{}_{gas} + [\Delta G(X^+)_{sol} - \Delta G(X)_{sol}]$$

Since we did not undertake full geometry optimization or include solvent effects in the calculations, ΔG was not actually determined and some approximations were necessary. Thus, we assume that the difference in the solvation free energy of X$^+$ and X is constant ($\Delta G(X^+)_{sol} - \Delta G(X)_{sol} = K$) and $\Delta G^{ox}{}_{gas} = \Delta G_{trans,rot,vib} + \Delta G_{el} \approx \Delta G_{el} \approx -\epsilon_{HOMO}$ (from Koopmans' theorem), so that

$$E°_{NHE} = \Delta G^{ox}{}_{sol} \approx \Delta G^{ox}{}_{gas} + K \approx -\epsilon_{HOMO} + K$$

A plot of $E°_{NHE}$ vs $-\epsilon_{HOMO}$ then gives

$$E°_{NHE} = A(-\epsilon_{HOMO}) + K$$

where A should approach 1 and K is a measure of the different solvation energies of X$^+$ and X. It is known that in fundamental density functional theory Koopmans'

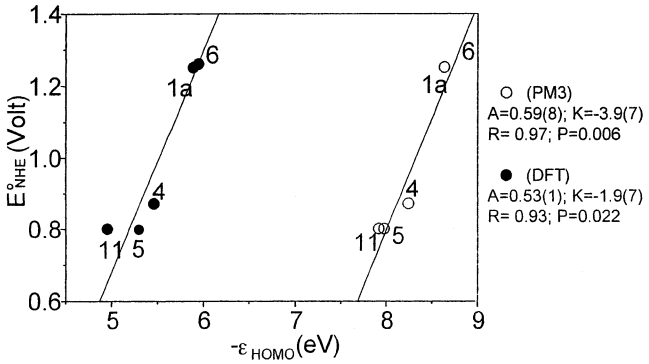

Figure 10. Plot of $E°_{NHE}$ vs $-\epsilon_{HOMO}$ for the semiempirical methods PM3 (○) and DFT (●). The solid lines show the best fit ($E°_{NHE} = A(-\epsilon_{HOMO}) + K$); the relative parameters are also indicated.

theorem would be *exact*.[20] Nonetheless, in theoretical chemistry it is still open to debate whether DFT orbital energies can be used in connection with Koopmans' theorem or for any other FMO theory considerations; indeed, it has often been claimed that DFT orbital energies have no physical meaning. On the other hand, it was recently concluded that DFT orbitals do indeed have physical meaning and are expected to be more suitable than Hartree−Fock (HF) orbitals for use in qualitative molecular orbital theory.[21] Also, it has been demonstrated that DFT orbitals behave similarly to HF orbitals, and the use of a scaling factor for the quantitative interpretation of both occupied and virtual DFT orbitals has been proposed.[22] This has been found to be true also in the case of transition-metal-containing complexes.[22]

Vertical ionization energies have been calculated for the dimeric species **4**−**6**, and a linear relationship between them and the energy of the HOMOs was found. The plot of $E°_{NHE}$ vs $-\epsilon_{HOMO}$ is shown in Figure 10 together with the best linear fit, indicating the reliability of the approximations done.

The slope of the best fit approaches 1 for the data obtained with both DFT and PM3 methods, in both cases closely approximating the experimental data ($R = 0.97$, $P = 0.006$[23] for PM3 and $R = 0.93$, $P = 0.022$ for DFT). Indeed, the slopes are parallel ($A = 0.59(8)$ for PM3 and 0.53(1) for DFT), even though the energies of the HOMOs evaluated by PM3 are rigidly shifted by ∼−3 eV (which gives rise to $K = -3.9(7)$ eV for PM3 vs −1.9(7) eV for DFT). When DFT data on ferrocene are included (the best linear fit has the parameters $A = 0.56(2)$, $K = -2(1)$), a greater departure from the linear fit is obtained ($R = 0.80$, $P = 0.058$), suggesting that the approximation to treat the difference of solvation energy as a constant is not rigorously valid in the case of molecules belonging to different structural classes. Indeed, if one includes only the data for the three related dimers **4**−**6**, the slope of the best fit is closer to 1, with a minor deviation from the best linear fit ($A = 0.73(7)$, $K = -3.1(4)$ and $R = 0.99$, $P = 0.069$). From DFT we obtain $K = \Delta G(X^+)_{sol} - \Delta G(X)_{sol} \approx -2$ eV ≈ -192 kJ/mol; this value is correctly negative and has the right order of magnitude compared with that recently obtained[24] by DFT for $Cp_2Fe_2S_4$, which is dimensionally comparable with our complexes.

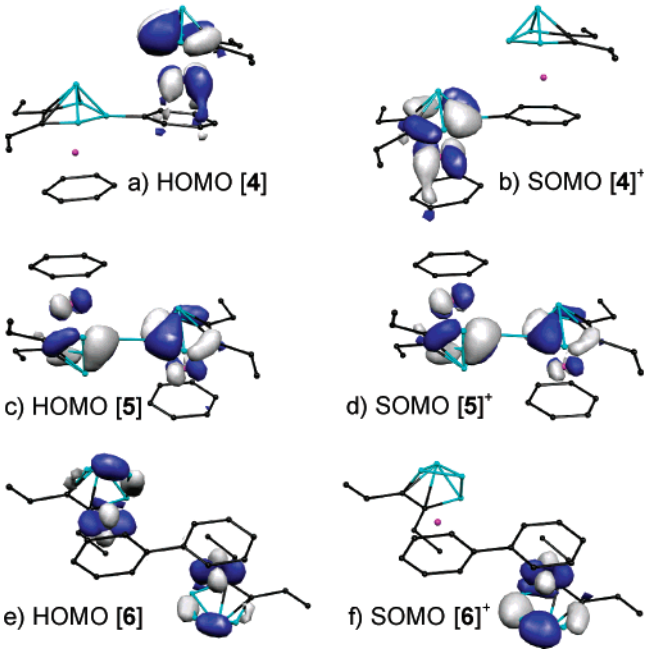

Figure 11. HOMOs of complexes **4**−**6** and SOMOs of the related cations, as obtained from B3LYP calculations.

To explore the extent of metal−metal interactions, we analyzed the composition of the HOMOs of neutral **4**−**6** and the SOMOs of their cations, shown in Figure 11.

In the asymmetric dimer **4** the separation between the two oxidation processes is 0.56 V, a value that, as noted earlier, one might interpret as an indication of high electronic interaction between the two ferracarborane subunits. However, according to our calculations both the HOMO of **4** and the SOMO of [**4**]$^+$ are completely localized on different iron sites (Figure 11a,b). More precisely, the HOMO is localized on the unsubstituted cluster and is destabilized in energy with respect to the HOMO of **1a**, by the antibonding interaction with the attached carborane.[25] As a result, the removal of one electron is made easier with respect to **1a** (0.63 V for **4** vs 1.01 for **1a**), as was also experimentally observed in complexes **2** and **3**.

As evidenced by the composition of the orbitals, the subsequent oxidations of **4** involve the removal of one electron from the other iron site. Consequently, we conclude that the observed difference in the redox potential values is actually due to the different inductive effects of the respective local coordinations, and hence **4** must be assigned as Robin−Day class I rather than class III. As noted earlier, **5** also exhibits two one-electron oxidations, each evidently accompanied by chemical changes, with a separation between the two anodic peaks of ca. 0.2 V at the highest scan rate. Also

(20) (a) Parr, R. G.; Yang, W. *Density-Functional Theory of Atoms and Molecules*; Oxford University Press: New York, 1989. (b) Koch, W.; Holthausen, M. C. *A Chemist's Guide to Density Functional Theory*; Wiley-VCH: Weinheim, Germany, 2000.

(21) Baerends, E. J.; Gritsenko, O. V. *J. Phys. Chem. A* **1997**, *101*, 5383.

(22) Stowasser, R.; Hoffmann, R. *J. Am. Chem. Soc.* **1999**, *121*, 3414.

(23) *P* has its usual statistical meaning as "the probability of obtaining the correlation *R* when the data are uncorrelated". In our cases the higher value of *P* indicates a probability of 2%.

(24) Blasco, S.; Demachy, I.; Jean, Y.; Lledos, A. *New J. Chem.* **2001**, *25*, 611.

(25) The destabilization is not apparent in the drawings in Figure 11, owing to the cutoff that was adopted for purposes of clarity.

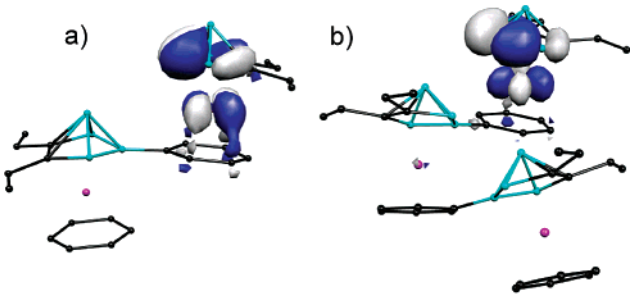

Figure 12. HOMOs of **4** (a) and **11** (b), showing orbitals strongly localized on the same iron center.

in this case the redox potential for the change **5**/[**5**]$^+$ is cathodically shifted with respect to the oxidation of **1a** (0.56 V for **5** vs 1.01 V for **1a**). This can be ascribed to the antibonding character of the interaction between the carborane units. According to our calculations, both the HOMO of **5** and the SOMO of [**5**]$^+$ are delocalized on the two iron sites (Figure 11c,d). This phenomenon is not unexpected for these complexes, given the strong contribution by the $R_2C_2B_4H_4^{2-}$ unit to the frontier orbital. Hence, the subsequent oxidations of **5** involve the succeeding formation of $Fe^{2.5}-Fe^{2.5}$ and $Fe^{III}-Fe^{III}$ systems from the starting $Fe^{II}-Fe^{II}$, and **5** must be assigned as Robin−Day class II.

The redox potential for complex **6** is virtually unchanged from that of **1a** (1.02 V for **6** vs 1.01 V for **1a**), indicating the absence of any significant interaction between the two monomeric units. Actually, the HOMO of **6** is delocalized on both iron sites (Figure 11e) while the SOMO of [**6**]$^+$ is localized (Figure 11f). As in the case of **4** and **5**, HOMO and HOMO-1 of **6** are the symmetric and asymmetric combination of iron-centered orbitals. The energy difference between these orbitals is the lowest in the series of complexes **4**−**6** (0.12 eV for **6** vs 0.63 and 0.31 eV for **4** and **5**, respectively), indicating a weak interaction between the two iron sites via the diphenyl chain; the 80° torsion angle between the two phenyl rings no doubt seriously inhibits electronic communication. The theoretical results show that, despite the existence of an interaction pathway, the electron relaxation that follows the oxidation process makes the cationic species [**6**]$^+$ valence trapped, as shown by the localized composition of the SOMO.

Finally, in the trimeric complex **11**, which is structurally related to **4**, the HOMO is similarly localized and centered on the corresponding subunit: i.e., that lacking an attached phenyl substituent on the carborane cage (Figure 12b). We therefore conclude that, as in **4**, the oxidation processes in **11** are localized on the individual subunits, with the separation of $E°$ attributed mainly to the different metal coordination environments.

Thus, it appears that effective communication between the iron centers requires symmetric linkage of the carborane clusters; electron delocalization via the diphenyl ligand is insufficient to restrain valence trapping in the mixed-valence species, while nonsymmetric phenyl−carborane linkages do not provide suitable electronic communication pathways in these systems.

Conclusions

In this study the electrochemical behavior of a structurally varied series of ferracarboranes ranging from mono- to trinuclear species has been coupled to a related theoretical investigation. The reliability of both DFT and PM3 calculations is supported by good agreement between the optimized and experimental structure of **1a**, by the well-reproduced trend of the redox potentials, and by the consistency of the two different methods of calculation. Data supporting the presence of metal−metal interactions have been found for the symmetric complexes **5** and **6**, while the orbital energy gap in **4** and **11** is ascribed to asymmetry. This study further underlines the strong electron-donating nature of the $Et_2C_2B_4H_4^{2-}$ ligand[4−7] and its ability to stabilize Fe^{III}−arene binding.[5a,b] The relatively small electronic communication between the iron centers in most of these d^5-d^6 $Fe^{III}-Fe^{II}$ systems (notably excepting the thiophene-bridged complex **10**) is in line with earlier observations on arene-linked FeC_2B_4 clusters and contrasts sharply with the high degree of delocalization that has been noted in fulvalene-linked d^6-d^7 ($Co^{III}-Co^{II}$) bis(cobaltacarboranes).[4] The question then is whether other hydrocarbon-linked $Co^{III}-Co^{II}$ carborane-based systems will follow the latter pattern and similarly behave as class III (highly delocalized) mixed-valence species. Current work in our laboratories is addressing this issue and will be reported in due course.

Acknowledgment. P. Z. gratefully acknowledges financial support from the University of Siena (PAR 2001), and F.F.d.B. thanks the *Access to Research Infrastructure Action of the Improving Human Potential Program* of the EC, for a grant to visit CESCA-CEPBA. Synthetic work conducted at the University of Virginia was generously supported by a grant (Grant No. CHE-9980708) from the National Science Foundation (U.S.) to R.N.G. We also wish to thank the reviewers for helpful comments and suggestions.

Supporting Information Available: Molecular structures of independent molecules in **1a** and a table of selected structural data from PM3 and DFT optimization and X-ray crystallography of **1a.** This material is available free of charge via the Internet at http://pubs.acs.org.

OM0201617